Embedded atom method potentials for Al-Pd-Mn phases

Daniel Schopf,[1,*] Peter Brommer,[1,2] Benjamin Frigan,[1] and Hans-Rainer Trebin[1]

[1]*Institut für Theoretische und Angewandte Physik (ITAP), Universität Stuttgart, Pfaffenwaldring 57, DE-70569 Stuttgart, Germany*

[2]*Département de Physique et Regroupement Québécois sur les Matériaux de Pointe (RQMP), Université de Montréal, C.P. 6128, Succursale Centre-Ville, Montréal, Québec, Canada H3C 3J7*

(Received 16 September 2011; revised manuscript received 19 December 2011; published 3 February 2012)

A novel embedded atom method (EAM) potential for the Ξ phases of Al-Pd-Mn has been determined with the force-matching method. Different combinations of analytic functions were tested for the pair and transfer part. The best results are obtained if one allows for oscillations on two different length scales. These potentials stabilize structure models of the Ξ phases and describe their energy with high accuracy. Simulations at temperatures up to 1200 K show very good agreement with *ab initio* results with respect to stability and dynamics of the system.

DOI: 10.1103/PhysRevB.85.054201 PACS number(s): 34.20.Cf, 02.70.Ns, 02.60.Pn

I. INTRODUCTION

The ternary intermetallic system Al-Pd-Mn has been of great interest in the last years, because it forms a high number of complex metallic alloy compounds (CMAs). In this paper, we focus on the Ξ phases, which are approximants of a decagonal quasicrystal with a lattice constant of 1.6 nm in the periodic direction. Under plastic deformation, these phases show a novel type of dislocations, so-called metadislocations, which were first described by Klein *et al.*[1]

Ab initio studies of these metadislocations, even with fast codes using density functional theory like VASP,[2,3] are currently unfeasible. Their spatial extent is about 200 Å and they involve more than 10 000 atoms—impossible to simulate even with state of the art *ab initio* programs.

With classical molecular dynamics (MD) it is easily possible to simulate structures with millions of atoms in reasonable time. The treatment of atoms as point masses interacting with an effective potential allows for microscopic insight into many processes on the atomic scale. The ability to control almost any aspect of the simulation can be used for optimizing the structure, determining physical properties or explaining physical phenomena in detail.

However, obtaining an effective potential for classical molecular dynamics is not straightforward. In order to extract reliable results, a potential has to be adjusted to the specific physical conditions considered. These can be, for example, high pressures, strain, surfaces, or phase boundaries. A common way is to fit a potential such that it reproduces experimental data like lattice constants, cohesive, and surface energies[4,5] or simply combining pure element potentials into an alloy potential.

For ternary systems, like Al-Pd-Mn, establishing a potential with these approaches is very challenging. The small number of available experimental data is not enough to fit reliable effective potentials. Hence, to obtain a potential that can be used for structure analysis and optimization, we apply the force-matching method[6] using the POTFIT package.[7,8] In the force-matching method, results from *ab initio* simulations are used as reference data to adjust the parameters of a potential. This not only dramatically increases the amount of information available for fitting (the total number of data points can easily reach several thousands). Also, if the reference data is found to be insufficient, more pertinent reference data can be generated at relatively low cost. This makes it possible to create realistic potentials for binary or ternary systems. In our case, we used forces on individual atoms, the cohesive energy and stresses on the unit cells to fit a reliable potential.

In Sec. II, we describe the interaction model used in this research. The fitting procedure using the force-matching method is presented in Sec. III, the reference data used are given in Sec. IV. The results will be discussed in detail in Sec. V.

II. EAM POTENTIALS

A common way to describe atomic interactions in metals is the *embedded atom method* (EAM).[9] It implicitly includes many-body interactions by a term that depends on the environment of every atom. The potential energy of a system described with the EAM method can be written as

$$E_{\mathrm{pot}} = \frac{1}{2}\sum_{\substack{i,j\\ j\neq i}} \Phi_{ij}(r_{ij}) + \sum_i F_i(n_i) \tag{1}$$

$$\text{with} \quad n_i = \sum_{j\neq i} \rho_j(r_{ij}). \tag{2}$$

The first term in Eq. (1) represents the pair interactions between atoms i and j at a distance $r_{ij} = |\boldsymbol{r}_j - \boldsymbol{r}_i|$. The function $F_i(n_i)$ is the embedding energy of atom i in the host density n_i. This density n_i (2) is calculated as the sum over contributions from the neighboring atoms, with ρ_j being the transfer function of atom j. It does not represent an actual physical density; n_i is a purely empirical quantity.

For the pair and transfer part, we have tested three different combinations of analytic functions as model potentials. Potential I has oscillations in the pair potential but not in the transfer function. In contrast, potential II has oscillations only in the transfer function. Finally, a third potential has oscillations in both functions.

For the simple pair potential without oscillations, we chose a Morse potential. It has a single minimum and is used in model II only:

$$\Phi(r) = \Psi\left(\frac{r-r_c}{h}\right) D_e\{(1-e^{-a(r-r_e)})^2 - 1\}. \tag{3}$$

Ψ is a cutoff function, where the free parameters r_c and h describe the cutoff radius and the smoothing of the potential. The remaining parameters are D_e, a, and r_e; D_e is the depth of the potential minimum, r_e the equilibrium distance and a the width of the potential minimum. The pair potential function with oscillations is adopted from Mihalkovič *et al.*:[10]

$$\Phi(r) = \Psi\left(\frac{r - r_c}{h}\right)\left[\frac{C_1}{r^{\eta_1}} + \frac{C_2}{r^{\eta_2}}\cos(kr + \varphi)\right]. \quad (4)$$

This "empirical oscillating pair potential" (EOPP) has been used in various works on complex metallic alloys and quasicrystals,[11–13] as it provides great flexibility. The first term of Eq. (4) with the parameters C_1 and η_1 controls the short-range repulsion. The second term is responsible for the damping (C_2, η_2) of the oscillations with the frequency k.

The cutoff function $\Psi(x)$ is defined by

$$\Psi(x) = \frac{x^4}{1 + x^4} \quad (5)$$

for $x < 0$ and $\Psi(x) \equiv 0$ for $x \geqslant 0$. This function guarantees that the potential functions, as well as their derivatives up to the second order, approach zero smoothly at the cutoff distance r_c.

Two different analytic forms were used as transfer functions; one allows for oscillations, the other one does not. The latter one is a simple exponential decay frequently used in established EAM potentials:[5,14,15]

$$\rho(r) = \alpha \exp(-\beta r), \quad (6)$$

where α is the amplitude and β is the decay constant. This function is used in model I. For models II and III, we used an oscillating transfer function, which is taken from Ref. 16:

$$\rho(r) = \Psi\left(\frac{r - r_c}{h}\right)\frac{1 + a_1\cos(\alpha r) + a_2\sin(\alpha r)}{r^{\beta}}. \quad (7)$$

The four free parameters are a_1, a_2, α, and β, where a_1 and a_2 determine the amplitude of the oscillations, α is the wave vector and β controls the decay.

The embedding function $F(n)$ was adopted from Ref. 14. It is based on the general equation of state from Rose *et al.*[17] The original form is given as

$$F(n) = F_0\left[\frac{q}{q - p}\left(\frac{n}{n_e}\right)^p - \frac{p}{q - p}\left(\frac{n}{n_e}\right)^q\right] + F_1\frac{n}{n_e}. \quad (8)$$

The parameters in this function are F_0, F_1, p, q, and n_e. p and q are real values and n_e is the equilibrium density. In this paper, we use this function in the limit $p \to q$ and chose $n_e = 1$:

$$F(n) = F_0\,[1 - q\ln n]\,n^q + F_1 n, \quad (9)$$

because the original form is numerically unstable with our optimization algorithms.

The number of free parameters of our three potential models is comparatively large. The nonoscillating (oscillating) pair potential has three (six) parameters, and the non-oscillating (oscillating) transfer function requires two (four) values. All models share the embedding function with three free parameters. Every pair and transfer function has one additional parameter h for the cutoff function Ψ. The cutoff radius r_c is kept fixed at 7 Å. In a ternary system like Al-Pd-Mn with 12 potential functions, this adds up to a total number of 60, 48, and 66 parameters for the models I, II, and III, respectively.

TABLE I. Binary structures ($T = 0$) used to fit the potentials, with their corresponding Pearson symbol.

Al-Mn structures	Al-Pd structures
$Al_{10}Mn_3$.*hP*26	AlPd.*cP*8
$Al_{11}Mn_4$.*aP*15	$Al_{21}Pd_8$.*tI*116
$Al_{12}Mn$.*cI*26	Al_3Pd_2.*hP*5
Al_6Mn.*oC*28	
AlMn.*tP*4	

III. FITTING PROCEDURE

All force-matching was performed with the POTFIT package of Brommer and Gähler,[7,8] which has previously been used to optimize tabulated pair and EAM potentials. For this work, its capabilities were extended to analytic potential models.

All free parameters of the analytic functions were fitted to an *ab initio* reference database containing relaxed ($T = 0$) structures, snapshots from *ab initio* MD simulations at higher temperatures and a few strained samples (see Tables I and II). All *ab initio* calculations were performed with the Vienna *Ab Initio* Simulation Package (VASP)[2,3] using the generalized gradient approximation (GGA) and the projector augmented wave (PAW) method.[18]

Two different optimization algorithms were used to fit the potentials. They both minimize the sum of squares defined by

$$Z = \sum \omega_E|\Delta E|^2 + \sum|\Delta F|^2 + \sum \omega_S|\Delta S|^2, \quad (10)$$

where ΔE, ΔF, and ΔS are the energy, force and stress residuals. These deviations are calculated as the difference of the *ab initio* and the EAM value, e.g.,

$$\Delta E = E_{\text{EAM}} - E_{\text{ab initio}}.$$

TABLE II. Ternary structures used to fit the potentials and their *ab initio* formation enthalpy ΔH.

	Number of atoms	ΔH (eV/atom)
$T = 0$	$Al_{92}Pd_{28}Mn_{10}$[a]	−0.512
	$Al_{92}Pd_{28}Mn_8$[a]	−0.485
	$Al_{112}Pd_{36}Mn_6$[b]	−0.526
	$Al_{114}Pd_{34}Mn_6$[b]	−0.503
	$Al_{112}Pd_{34}Mn_6$[b]	−0.512
	$Al_{110+x}Pd_{32}Mn_8$[b]	see Sec. V A
	$Al_{124}Pd_8Mn_{24}$[b,c]	−0.297
	$Al_{147}Pd_{43}Mn_{18}$[b]	−0.485
	$Al_{294}Pd_{88}Mn_{16}$[b]	−0.491
$T > 0$	$Al_{92}Pd_{28}Mn_8$[a,d]	–
	$Al_{92}Pd_{28}Mn_{10}$[a] (1500 K)	–

[a]Structure generated from canonical cell tiling.[21]
[b]From structure optimization.
[c]T-Al-Pd-Mn, see Sec. IV.
[d]From several MD runs at 600, 1100, and 1800 K with small strains.

ω_E and ω_S are global weights for the energies and stresses. $\omega_E = 22\,500$ was chosen to obtain potentials that yield very precise energies, but also reasonable forces. For configurations with about 150 atoms, this effectively weighs the energies with a factor of approximately 50. The stress weight ω_S was set to 750, so that the total weight of the six stress tensor components per configuration is approximately equal to ten times the weight of all forces in one configuration.

The first optimization algorithm used is simulated annealing.[19] It is based on the Metropolis criterion, where a decrease in the target function Z is always accepted and an increase only with a probability $P = e^{-\Delta Z/T}$. This allows the algorithm to escape local minima. The artificial temperature T is steadily decreased during the optimization. To ensure that the fit converged to the global minimum, the optimization was restarted with a high temperature several times. Subsequently, a conjugate gradient based method[20] was applied to converge to the final optimum. During the fitting procedure, all parameters were confined to a predefined range by use of numerical punishments.

IV. REFERENCE DATA

The structures used as reference data are shown in Tables I and II. There are 119 configurations with a total of 16 103 atoms. The number of reference data points is 49 340. They consist of 48 309 forces, 119 energies, and 714 stresses.

In addition to the binary and ternary structures, one reference configuration for each of the pure elements was also included. These were, in detail, Al.*cF*4, Pd.*cF*4, and Mn.*cI*58. This was done to get reliable reference points for the calculation of the enthalpy of formation.

All atomic configurations from binary systems (see Table I) were taken from the alloy database of Widom *et al.*[22] and have been fully relaxed with *ab initio* methods. They were chosen to provide more data for the Pd-Pd and Mn-Mn interactions. Magnetism was not included in our *ab initio* calculation; it was shown that the manganese atoms in the Ξ phases are nonmagnetic.[23] Because the structures we want to investigate are on the aluminum-rich side of the phase diagram, there is only little data for the Mn-Pd interaction.

The reference configurations for the Ξ phases are from different sources. The structures in Table II denoted with superscript a were taken from the alloy database.[22] They were generated with the canonical cell tiling,[21] which creates hypothetical models by decorating a tiling with clusters. To compensate for the low amount of manganese in these samples and the hence resulting lack of data, five of the aluminum atoms were replaced by manganese in some configurations. *Ab initio* molecular dynamics simulations with VASP[2,3] were run with these samples at 600, 1100, and 1800 K to obtain different local atomic configurations. These calculations were done in the generalized gradient approximation (GGA) with PAW potentials.[18]

At the same time, *ab initio* structure optimization was carried out for two of the Ξ phases. Particularly, this were the Ξ phase with the smallest unit cell, which contains about 152 atoms and is called ξ and the next bigger one, containing about 304 atoms, which is called ξ'. All structures generated in the course of this optimization are denoted in Table II by superscript b.

TABLE III. Root mean square errors after the optimization for forces (in meV/Å), energies (in meV/atom), and stresses (in kPa). These data are calculated with the reference configurations used for fitting the potentials.

RMS errors for	Model I	Model II	Model III
forces	265.63	221.40	220.07
energies	19.36	14.49	12.53
stresses	99.99	76.83	98.30

To judge the stability of these structures, their energy is compared to a mixture of competing phases, the convex hull. This hull, defined over a ternary phase diagram, contains the cohesive energies of all stable compounds as vertices. If the energy of a structure is above this convex hull, it could decompose into the neighboring structures and thus lower its energy. If the energy of a new structure is below the convex hull, it is considered to be thermodynamically stable. The structures that define the convex hull for the Ξ phases, are T-AlPdMn, $Al_{12}Mn$, $Al_{21}Pd_8$, and Al_3Pd_2. They have also been included in the reference database. A detailed description of these phases and the convex hull is given in Ref. 24.

V. RESULTS

We determined parameters for all three potential models from the reference data described above. The root mean square (RMS) errors for forces, energies, and stresses after the optimization are in the same order of magnitude for all models (see Table III). While model III has the smallest errors for forces and energies, model I has the biggest errors for all three quantities. Model II has the smallest stress deviations. While the force error for model I is about 20% larger than the one for model III, the energy error is significantly larger with about 50% difference.

A graphical representation of these errors can be seen in Fig. 1. The scatter plots in the upper row display the energies

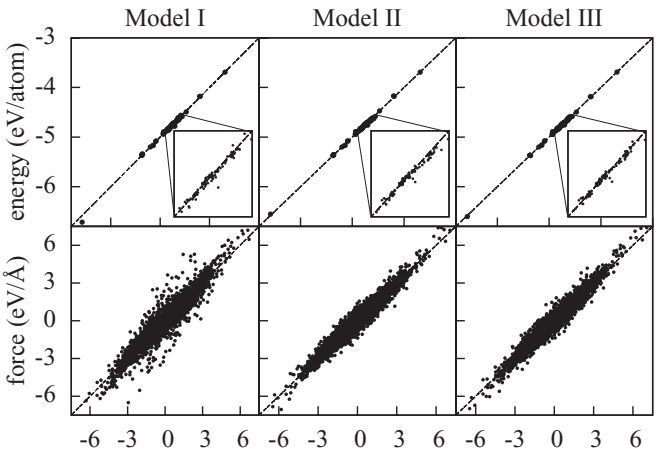

FIG. 1. Scatter plot for energies and forces with the EAM values on the vertical axis and the *ab initio* reference data on the horizontal axis. The insets are magnified by a factor 4.5.

TABLE IV. Root mean square errors for forces (in meV/Å), energies (in meV/atom), and stresses (in kPa). These data are calculated with test data, containing only structures that were not included in the optimization process.

RMS errors for	Model I	Model II	Model III
forces	141.90	131.90	130.46
energies	10.42	10.47	10.28
stresses	32.39	23.76	36.89

of the reference data. Forces are shown in the lower row. The range of the force plots is due to the many high-temperature MD simulations that are included in the reference data. The forces therein can become very large because of the short interatomic distances that may occur at these temperatures.

These errors cannot solely be used to judge the quality and transferability of the potentials. For that purpose, another set of *ab initio* data has been extracted from the structure optimization. It has not been included in the reference data and can be used to determine the transferability of the different potentials. The same errors as before have been calculated and can be seen in Table IV. As with the reference data, model III has the lowest force and energy errors. The relative error of the energy is about 0.2%, for stresses about 5%, and 550% for forces. This is due to the fact that all configurations in these test data are ground-state structures and therefore only contain very small forces.

The errors for the test data in Table IV are smaller than those of the reference configurations in Table III, because there are only ground states included and no high temperature MD runs.

Based upon these simple energy and force considerations, all the potential models appear to be of similar quality. Model III, however, should be slightly superior to the other two potentials. Further tests are necessary to determine the performance of the potentials in different situations. They will be presented in Sec. V B.

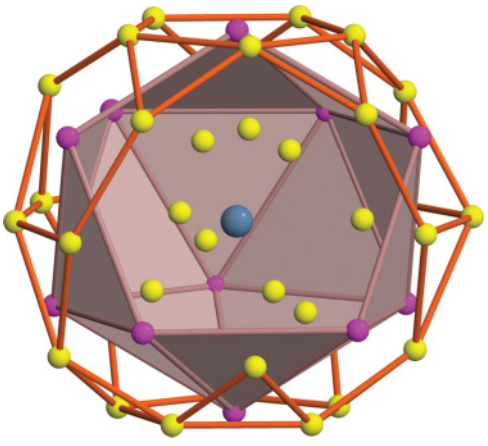

FIG. 2. (Color online) Detailed structure of the pseudo-Mackay icosahedral cluster. A few atoms of the second and third shell are omitted to see the central atom and the aluminum atoms in the first shell. The icosahedron and icosidodecahedron are indicated by planes and bars, respectively. The central atom is manganese. Aluminum atoms are depicted in yellow (light gray) and palladium atoms in magenta (dark gray).

TABLE V. Cohesive energies (in eV/atom) of different optimized configurations for the ξ phase. The energy differences ΔE between the *ab initio* calculations and the respective model are given in meV/atom.

Number of atoms per PMI	$E_{\text{ab initio}}$ (eV/atom)	ΔE (meV/atom)		
		Model I	Model II	Model III
8	−4.753	−13	−12	−20
8.25	−4.755	−6	−7	−13
8.5	−4.756	−1	−3	−5
8.75	−4.757	+3	+2	+2
9	−4.755	+4	+4	+3
9.25	−4.747	+1	+1	+1
9.5	−4.741	+1	+0	+2
9.75	−4.731	−6	−5	−2
10	−4.731	+0	+2	+4
10.25	−4.714	−12	−12	−5
10.5	−4.704	−15	−17	−7
10.75	−4.692	−19	−21	−13
11	−4.683	−22	−24	−17

A. Structure refinement

In Ref. 24, the structure of the Ξ phases of Al-Pd-Mn has been optimized by energy minimization in *ab initio* and molecular dynamics simulations. We use several of the structures tested there to judge the quality of the optimized potentials. The Ξ phases consist of columns of pseudo-Mackay icosahedral clusters (PMIs),[25] a slight deviation of the famous Mackay icosahedron.[26]

Every PMI cluster consists of a single atom at the center with a first shell of an experimentally poorly determined number of aluminum atoms. The second shell is an icosahedron of 12 transition metal atoms and the outer shell an icosidodecahedron of 30 aluminum atoms, see Fig. 2. Almost all atoms of the Ξ phases belong to these clusters. It is difficult to measure the exact number of atoms in the first shell because aluminum atoms are hard to observe in diffraction experiments.

For the lowest quasicrystal approximant, the ξ phase, there are four PMI clusters in one unit cell. Several different occupancies of aluminum atoms in the first shell were tested in Ref. 24. Each configuration was denoted by a single number, giving the average number of aluminum atoms per cluster. Structures from eight up to eleven atoms per PMI were generated and tested.

TABLE VI. Cohesive energies (in eV/atom) of the four almost stable phases after relaxation. The energy differences ΔE are given in meV/atom. The composition is given in numbers of aluminum, palladium and manganese atoms, in this order. All configurations have nine aluminum atoms in the inner shell of the PMI clusters.

composition	$E_{\text{ab initio}}$ (eV/atom)	ΔE (meV/atom)		
		Model I	Model II	Model III
ξ-228–64–12	−4.702	−5	+4	0
ξ-224–68–12	−4.748	+1	+7	+4
ξ'-228–64–12	−4.703	−5	+3	+1
ξ'-224–68–12	−4.748	+1	+5	+5

TABLE VII. Cohesive energies for different phases in the Al-Pd-Mn system. All energies and energy differences are given in eV/atom. The mean square displacements (Δx) after relaxation are given in Å/atom. A displacement of 0 means the value is smaller than 10^{-4} Å/atom.

System	$E_{\text{ab initio}}$ E (eV/atom)	Model I			Model II			Model III		
		E_{EAM}	ΔE	Δx	E_{EAM}	ΔE	Δx	E_{EAM}	ΔE	Δx
AlPd.*cP*2 (B2)	−5.330	−5.430	−0.100	0	−5.503	−0.173	0	−5.445	−0.115	0
$AlPd_3$.*cF*16 ($D0_3$)	−5.236	−5.426	−0.190	0	−5.424	−0.188	0	−5.430	−0.194	0
Al_3Pd.*tI*8 ($D0_{22}$)	−4.421	−4.546	−0.125	0	−4.540	−0.119	0	−4.560	−0.139	0
Al_3Pd.*cP*4 ($L1_2$)	−4.609	−4.647	−0.038	0.13	−4.651	−0.042	0.17	−4.650	−0.041	0.17
Al_3Mn.*tI*8 ($D0_{22}$)	−5.132	−5.053	0.079	0.04	−5.129	0.003	0.01	−5.175	−0.043	0
Al_3Mn.*cP*4 ($L1_2$)	−5.032	−5.187	−0.155	0	−5.180	−0.148	0	−5.197	−0.165	0

The results with the different potential models can be seen in Table V. All structures were completely relaxed with *ab initio* methods, the corresponding *ab initio* energy is given in the second column. The energies of these configurations with the generated EAM potentials have been calculated after subsequent relaxation with the respective potentials. This relaxation causes small displacements of the atoms from their *ab initio* determined positions. For models I, these average displacements are 0.10 Å/atom, 0.08 Å/atom for model II, and 0.11 Å/atom for model III. This clearly shows that all potential models can stabilize the ground states of all structures that were generated.

All models are having difficulties with the energies of structures that contain less than nine or more than ten atoms in the inner shells of the PMI clusters. This may be an indication for the mechanical instability found during the structure optimization.[24] The energy of these structures is highly unfavorable; at elevated temperatures some atoms drifted from the outer shell to the inner shell or vice versa to achieve an inner shell with nine or ten aluminum atoms.

All energy differences between the *ab initio* and EAM calculations are smaller than 10 meV/atom for configurations ranging from 8.5 to 10 atoms per PMI cluster. This energy is considered a critical threshold for the accuracy of the potentials. Regarding the energy differences between the different structures, which are on the order of 1 meV/atom, all potentials can evidently distinguish between these different configurations.

The structure optimization in Ref. 24 yielded four almost stable structures, which are different from the ones shown in Table V. There, not only the atoms in the inner shell are varied, but also atoms not belonging to the PMI clusters. These alterations were not done in a systematic manner, the structures will be listed in tabular form. The amount of atoms for ξ- and ξ' phases is the same, only the arrangement of the PMI cluster columns is different. These structures were tested with the three different potentials. The results can be seen in Table VI. The two upper structures in this table are ξ phase, the two lower structures are ξ'.

After the relaxation with the effective potentials, all models show a very good agreement with the *ab initio* calculated energies. The mean displacements after the relaxation are again in the same order of magnitude as before, 0.11 Å/atom for model I, 0.08 Å/atom for model II, and 0.15 Å/atom for model III. Based on these pure energy comparisons, all three potential models seem to be of equal quality, with slight advantages for model III.

B. Tests

A force-matched potential is only useful if it can reproduce key quantities that were not directly included in the reference data. Here, we subjected the three potentials to a series of tests. The first test is whether the potential can stabilize the ξ phase even at elevated temperatures. As there was a large number of high-temperature *ab initio* MD simulations included in the optimization, the potentials should be able to preserve the structure of the ξ phase under these conditions. We carried out an *ab initio* MD simulation at 1200 K for 50 ps,[24] where the phase is still mechanically stable. In a time-averaged picture of the density, the atoms in the two outer shells of the PMI clusters did not move, but the atoms in the first shell showed some rotational degree of freedom.

All three models were able to stabilize the structure at this temperature. While models II and III give the same results as the *ab initio* calculation (see Ref. 24), model I shows additional degrees of freedom. In the time-averaged picture, the atoms forming the outer shell of the PMIs are not as steady as in the *ab initio* simulation. Also the atoms, which do not belong the these clusters, exhibit a density distribution that is twice as large as expected. This means that model I may have difficulties stabilizing the structure at even higher temperatures or against fluctuations in the local atomic arrangement.

For molecular dynamics simulations, the stabilization of different phases can be a problem. We checked some well-known phases for all three potential models with respect to cohesive energy and phase stability. The results can be seen in Table VII. All three potentials can stabilize the different phases. The deviation of the atomic positions after relaxation compared to the *ab initio* reference values is very small. The energies are reproduced with errors of under 200 meV/atom.

TABLE VIII. *Ab initio* energies (in eV/atom) and the differences for the effective potentials (in meV/atom) for the pure elements. These energies were used for the calculation of the formation enthalpies ΔH.

	$E_{\text{ab initio}}$ (eV/atom)	ΔE (meV/atom)		
		Model I	Model II	Model III
Al.*cF*4	−3.688	−5	−4	−3
Pd.*cF*4	−5.199	0	0	0
Mn.*cI*58	−8.964	+68	−7	+3

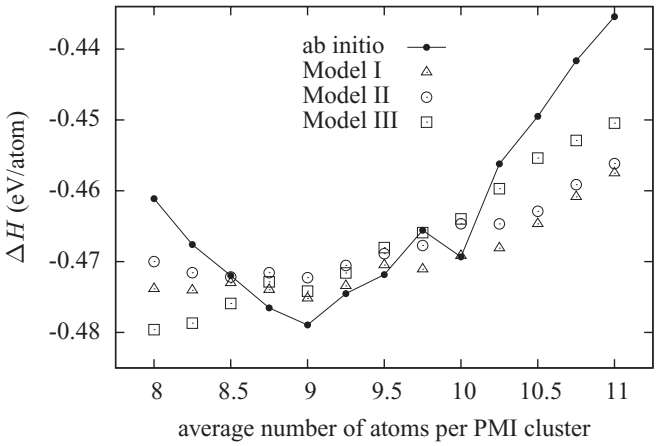

FIG. 3. Comparison of the *ab initio* formation enthalpy ΔH (in eV/atom) with the three potential models. The lines between the *ab initio* data points are added as a guide to the eye.

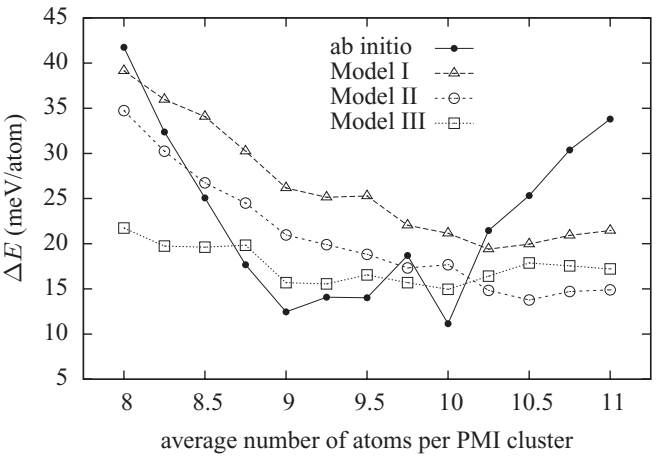

FIG. 4. Difference of the cohesive energy to the convex hull for different amounts of aluminum atoms in the inner shell of the PMI clusters. The data points for model I are shifted by +10 meV/atom and by +5 meV/atom for model II.

Another important test is the calculation of formation enthalpies ΔH with the potentials. ΔH is defined as the energy difference of a structure to the tie plane of the pure element energies. This has been calculated for all configurations in Tables V and VI. The reference energies are given in Table VIII. For the structures with different amounts of aluminum atoms in the inner shell of the PMI clusters, the results can be seen in Fig. 3. The deviations from the *ab initio* enthalpies are very similar to those from Table V. For less than 8.5 and more than 10 atoms in the inner shell of the PMI clusters, the enthalpies differ more than 10 meV/atom.

The enthalpies for the four almost stable structures are shown in Table IX. All three models give very accurate enthalpies with deviations all smaller than 10 meV/atom.

During the structure optimization a very long *ab initio* MD run with 50 000 steps at 1200 K was performed. Snapshots were taken from this simulation at different timesteps and quenched very rapidly. This has also been done with the EAM potentials. The results show a very good agreement for different snapshots. The structures only differ very slightly in atomic positions. While there is a steady offset of about 100 meV/atom in the energy for higher temperatures, the overall trend can clearly be followed. For lower temperatures and $T = 0$, the energies were in the same order as for the structures in Table V. There were no major differences for all three potential models.

To determine if a structure is thermodynamically stable, the energy difference of this structure to the convex hull is calculated. If this difference is negative, the structure is stable, otherwise it it unstable. For more details on the convex hull see Ref. 24. This energy difference has been calculated for all structures in Table V and is shown in Fig. 4.

For the sake of clarity, the data points of model I and II are shifted by +10 and +5 meV/atom. While these models show a clear decrease of the energy difference with increasing number of atoms inside the PMI cluster, model III has minima for nine and ten atoms, like the *ab initio* reference calculation. As this is the main criterion for performing a structure optimization, models I and II cannot be used for this purpose. Only model III is able to reproduce the shape of the *ab initio* calculation.

The melting point for the ξ phase has been determined with all three potential models. In MD simulations, the volume per atom has been calculated while the sample was heated from 950 to 1400 K. At the melting point, there is a jump in atomic volume, which corresponds to the melting transition. For model I, this was found at 1130 K, for model II, at 1370 K, and for model III, at 1300 K. With this method, the melting point is generally overestimated, due to the high heating rates. For the simulations, we chose a heating rate

TABLE IX. *Ab initio* formation enthalpies ΔH (in eV/atom) of the four almost stable phases and the differences for the effective potentials (in meV/atom) after relaxation. The composition is given in numbers of aluminum, palladium, and manganese atoms, in this order. All configurations have 9 aluminum atoms inside the PMI clusters.

composition	$\Delta H_{\text{ab initio}}$ (eV/atom)	$\Delta H_{\text{EAM}} - \Delta H_{\text{ab initio}}$ Model I	Model II	Model III
ξ-228–64–12	−0.488	−6	+1	−1
ξ-224–68–12	−0.513	0	+4	+3
ξ'-228–64–12	−0.488	−6	0	0
ξ'-224–68–12	−0.514	0	+2	+3

TABLE X. Elastic constants of ξ-Al-Pd-Mn in GPa.

	ab initio	Model I	Model II	Model III
C_{11}	175.79	255.25	244.66	200.98
C_{22}	192.75	269.79	246.74	193.61
C_{33}	227.46	243.53	246.64	160.57
C_{12}	58.76	158.83	145.57	102.76
C_{13}	67.85	146.75	146.78	92.95
C_{23}	56.34	151.19	146.51	107.04
C_{44}	72.54	42.57	42.42	42.77
C_{55}	67.77	41.46	47.19	46.66
C_{66}	71.25	48.51	48.21	43.76

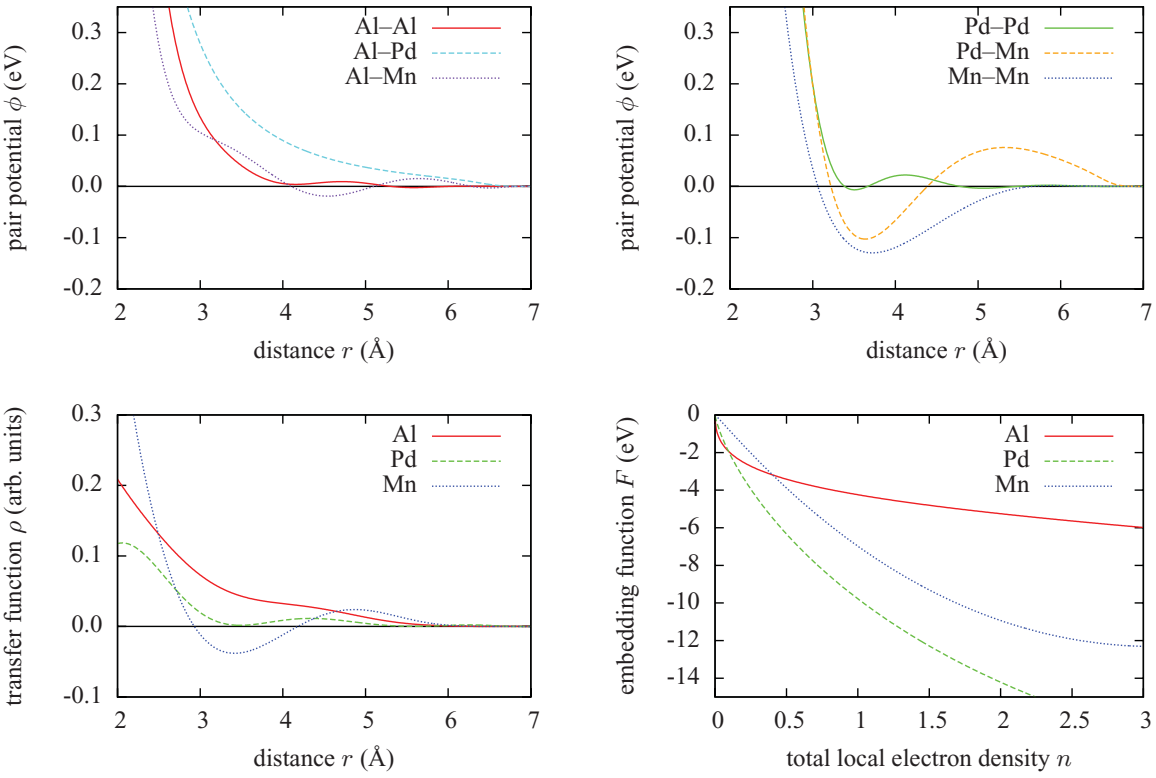

FIG. 5. (Color online) Plots of the 12 functions of the EAM potential (model III) for Al-Pd-Mn.

of 5×10^{-5} K per time step, this equals 5×10^{9} K/s. If one compares these temperatures with the experimental value of 1118 K, the value for the potential model I seem to be too low, model II and III are in the expected temperature range.

Another test we performed is the calculation of the elastic constants. All Ξ phases have an orthorhombic unit cell. The corresponding nine elastic constants were determined by examining the cohesive energy during homogeneous deformations of the sample.

The results with all three models (see Table X) show only very little agreement with the *ab initio* values. Only model III can reproduce C_{11} and C_{22}. All other elastic

TABLE XI. Parameters for the model III EAM potential with r in units of Å and $V(r)$ in eV.

EOPP pair function							
pair	C_1	η_1	C_2	η_2	k	φ	h
Al-Al	586.4805	7.6769	−0.0333	1.0012	3.7658	3.8484	1.3897
Al-Mn	338.7250	7.5484	−0.4212	1.9271	2.7530	0.0033	0.5000
Al-Pd	981.8107	9.1908	−89.9193	4.7322	0.2491	1.3235	0.6211
Mn-Mn	3.8460	19.9995	−44.5953	4.1469	1.2084	1.0115	1.5938
Mn-Pd	12.8931	3.4348	−90.3824	4.4851	1.6212	0.0005	0.5007
Pd-Pd	6625.3081	9.5962	99.8792	6.1164	3.8088	2.5086	0.5235
transfer function							
element	a_1	a_2	α	β	h		
Al	0.1317	0.0399	2.7507	2.3142	1.9995		
Mn	−1.5432	1.0321	1.6018	2.4154	1.9996		
Pd	0.4962	0.7317	2.9972	3.4308	0.5001		
embedding function							
element	F_0	F_1	q				
Al	−2.9403	0.5639	−1.3026				
Mn	−1.5862	1.3917	−5.3935				
Pd	−4.0016	0.9432	−5.7749				
cutoff radius $r_c = 7$ Å							

constants differ by up to a factor of three. The potentials are apparently not able to reproduce the shear stress. However, this behavior is to be expected, if one takes into account that these potentials were generated for energy minimization purposes. For other applications, like calculating mechanical properties, an extended database, containing enough data on shears, should be used. The only samples used for these potentials, that included deformations, were high-temperature *ab initio* MD snapshots. These were strained along either of the cartesian axes that are perpendicular to the periodic stacking axis of the quasicrystal. The corresponding elastic constants are C_{11} and C_{22}, which are the only ones correctly reproduced by model III.

This clearly shows that force matched potentials are limited in their applications. They give very accurate results regarding the energy and forces because they are tuned to these quantities. For other physical properties, like elastic constants, the potentials are less accurate.

VI. SUMMARY

The Al-Pd-Mn potentials presented are very well suited to model the energetics of the Ξ phases. They were obtained with the force-matching method, which is fitting the parameters to a large database of *ab initio* determined reference data. All three analytic potential models tested were able to reproduce the *ab initio* values of the energies with very high accuracy. The error sum of the fitting process for all three potentials is very similar, yet they show very different properties when used in MD simulations.

The differences of the models become visible when calculating energy differences like formation enthalpies or the convex hull. There, model III shows the smallest deviations and can reproduce the *ab initio* values with very high accuracy. The models I and II also give very good energies differences but cannot be used to predict the stability of a structure with the calculation of the convex hull. This indicates that oscillations on two length scales, like in model III, are necessary. However, the reasons for this are unclear. For further structure determination and analysis of the metadislocations in the Ξ phases, the model potential III will be used.

ACKNOWLEDGMENTS

We would like to thank Alejandro Santana Bonilla and Marek Mihalkovič for intensive discussions and providing some test and reference data. This project has been funded by the European Network of Excellence "Complex Metallic Alloys" (NMP3-CT-2005-500140) and by Deutsche Forschungsgemeinschaft, Paketantrag "Physical Properties of Complex Metallic Alloys, (PAK 36)," TR 154/24-2.

*Daniel.Schopf@itap.uni-stuttgart.de

[1] H. Klein, M. Feuerbacher, P. Schall, and K. Urban, Phys. Rev. Lett. **82**, 3468 (1999).
[2] G. Kresse and J. Hafner, Phys. Rev. B **47**, 558 (1993).
[3] G. Kresse and J. Furthmüller, Phys. Rev. B **54**, 11169 (1996).
[4] S. M. Foiles, M. I. Baskes, and M. S. Daw, Phys. Rev. B **33**, 7983 (1986).
[5] J. Mei, J. W. Davenport, and G. W. Fernando, Phys. Rev. B **43**, 4653 (1991).
[6] F. Ercolessi and J. B. Adams, Europhys. Lett. **26**, 583 (1994).
[7] P. Brommer and F. Gähler, Philos. Mag. **86**, 753 (2006).
[8] P. Brommer and F. Gähler, Modelling Simul. Mater. Sci. Eng. **15**, 295 (2007); [http://www.itap.physik.uni-stuttgart.de/∼imd/potfit].
[9] M. S. Daw and M. I. Baskes, Phys. Rev. Lett. **50**, 1285 (1983).
[10] M. Mihalkovič, C. L. Henley, M. Widom, and P. Ganesh, e-print arXiv:0802.2926v2 (unpublished).
[11] M. Mihalkovič, W. J. Zhu, C. L. Henley, and R. Phillips, Phys. Rev. B **53**, 9021 (1996).
[12] M. Mihalkovič, I. Al-Lehyani, E. Cockayne, C. L. Henley, N. Moghadam, J. A. Moriarty, Y. Wang, and M. Widom, Phys. Rev. B **65**, 104205 (2002).
[13] M. Krajci and J. Hafner, Phys. Rev. B **46**, 10669 (1992).
[14] R. A. Johnson and D. J. Oh, J. Mar. Res. **4**, 1195 (1989).
[15] R. Pasianot and E. J. Savino, Phys. Rev. B **45**, 12704 (1992).
[16] S. Chantasiriwan and F. Milstein, Phys. Rev. B **53**, 14080 (1996).
[17] J. H. Rose, J. R. Smith, F. Guinea, and J. Ferrante, Phys. Rev. B **29**, 2963 (1984).
[18] G. Kresse and D. Joubert, Phys. Rev. B **59**, 1758 (1999).
[19] S. Kirkpatrick, C. D. Gelatt, and M. P. Vecchi, Science **220**, 671 (1983).
[20] M. J. D. Powell, Comp. J. **7**, 303 (1965).
[21] C. L. Henley, Phys. Rev. B **43**, 993 (1991).
[22] M. Widom and M. Mihalkovič; [http://alloy.phys.cmu.edu].
[23] F. Hippert, V. Simonet, G. T. de Laissardière, M. Audier, and Y. Calvayrac, J. Phys. Condens. Matter **11**, 10419 (1999).
[24] B. Frigan, A. Santana, M. Engel, D. Schopf, H.-R. Trebin, and M. Mihalkovič, Phys. Rev. B **84**, 184203 (2011).
[25] W. Sun and K. Hiraga, Phil. Mag. A **73**, 951 (1996).
[26] A. L. Mackay, Acta Crystallogr. **15**, 916 (1962).